Modeling and Reduction of Radiated EMI in a GaN IC-Based Active Clamp Flyback Adapter

Juntao Yao, *Student Member, IEEE*, Yiming Li, *Student Member, IEEE*, Shuo Wang, *Fellow, IEEE*, Xiucheng Huang, and Xiaofeng Lyu, *Member, IEEE*

***Abstract*—This article first develops a radiated electromagnetic interference (EMI) model for a gallium nitride (GaN) integrated circuit (IC)-based active clamp flyback converter. Important capacitive couplings, which play a big role in the radiated EMI, are identified, extracted, and validated in the converter. The radiated EMI model is improved to characterize the impact of capacitive couplings. Based on the improved model, techniques to reduce capacitive couplings and the radiated EMI are proposed and experimentally validated.**

***Index Terms*—Active clamp, capacitive coupling, flyback converter, gallium nitride (GaN) device, radiated electromagnetic interference (EMI).**

I. Introduction

In MODERN power electronics, fast-switching gallium nitride (GaN) devices can operate at the switching frequencies higher than conventional Si MOSFETs, so they help significantly reduce the size of passive components and increase power density [1]–[5]. The active clamp flyback (ACF) converter is a ZVS soft-switching topology, which recycles the energy stored in leakage inductance [6], [7] to improve conversion efficiency. Working with GaN devices, the ACF converter operating at several hundred kHz to 1 MHz could be a game-changer for high-power-density and high-efficiency power adapters [8].

However, fast-switching GaN devices lead to high switching noise especially radiated EMI [6], [9]–[11]. Also, high power-density layout leads to near field couplings, which degrade the EMI filter performance [12]. Radiated EMI of a power converter has been analyzed in [9], [10], [13], and [14]: the long power cables attached to the power converter behave like an antenna [10], [13], [14] driven by the noise generated by the power converter; in isolated power converters, the antenna can be driven by the voltage difference between the primary ground (PGND) and the secondary ground (SGND) [9], [10], [13], [15], [16], which is mainly caused by the unbalanced transformer parasitics. Radiated EMI can be suppressed by reducing the common mode (CM) currents flowing between transformer primary and secondary windings. Techniques such as CM chokes with high-frequency (HF) lossy magnetic cores and coaxial shielding winding transformers can help reduce the radiated EMI [10], [14]; however, due to the parasitics such as parasitic capacitance and inductance, their HF performance has much to desire [12], [17]–[21]. In a high-power-density design, near field couplings can degrade the EMI filter performance, so it is important to investigate the couplings within converters [5], [22]–[24].

This article investigates the modeling and reduction of radiated EMI. Section II will develop a model for the radiated EMI. In Section II-A, a preliminary radiated EMI model will be first developed. In Section II-B, the impact of the capacitive couplings on the radiated EMI will be identified and analyzed. An improved radiated EMI model will be developed to characterize the impact of the capacitive couplings. In Section III, techniques to reduce capacitive couplings and the radiated EMI will be proposed and verified. The investigation in this article is based on a 60 W GaN integrated circuit (IC)-based ACF power adapter.

II. Development of the Radiated EMI Model Including Capacitive Couplings

Fig. 1(a) shows a GaN IC-based ACF power adapter above the ground. Fig. 1(b) shows the photograph of the prototype. The input and output voltages are 120 V AC and 20 V DC, respectively. The main and clamping switches, and gate drivers are integrated into Navitas Semiconductor's GaN ICs NV6117 and NV6115. The switching frequency is 450 kHz, and the switching slew rate in this ACF is 20 V/ns. The winding structure of the planar transformer has been optimized to minimize the conductive CM noise [6]. The lengths of the input and output cables are 0.8 m and 0.9 m, respectively. The load is a 6.67 Ω power resistor.

A. Preliminary Radiated EMI Model

The radiated EMI is mainly caused by the CM currents flowing on input and output cables. The differential mode (DM) currents of the converter do not significantly contribute to the radiated EMI [9]. Based on the substitution theory, SW_1 can be replaced with a voltage source V_{SW1}; SW_2 and SW_3 can be replaced with current sources I_{SW2} and I_{SW3} in Fig. 2. Based on

Manuscript received February 26, 2020; revised June 23, 2020; accepted August 20, 2020. Date of publication October 20, 2020; date of current version January 22, 2021. This work was supported by Navitas Semiconductor Inc. Recommended for publication by Associate Editor F. Luo. *(Corresponding author: Shuo Wang.)*

Juntao Yao, Yiming Li, and Shuo Wang are with the Department of Electrical and Computer Engineering, University of Florida, Gainesville, FL 32608-2538 USA (e-mail: juntaoyao@ufl.edu; brighturan@ufl.edu; shuo.wang@ece.ufl.edu).

Xiucheng Huang and Xiaofeng Lyu are with the Navitas Semiconductor Inc., El Segundo, CA 90245 USA (e-mail: xiucheng.huang@navitassemi.com; xiaofeng.lyu@navitassemi.com).

Color versions of one or more of the figures in this article are available online at https://ieeexplore.ieee.org.

Digital Object Identifier 10.1109/TPEL.2020.3032644

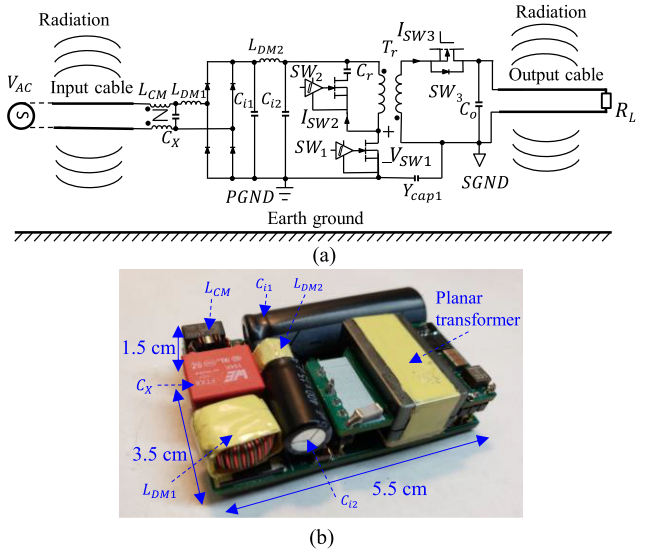

Fig. 1. GaN IC-based ACF power adapter with power cables attached (a) circuit. (b) Prototype photograph.

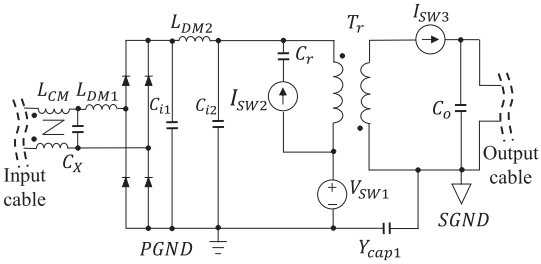

Fig. 2. EMI noise model of an ACF with switching devices substituted by voltage/current sources.

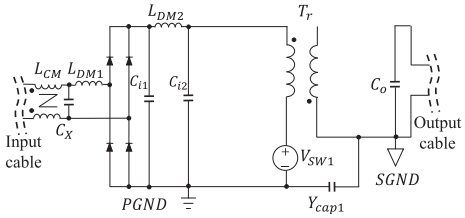

Fig. 3. EMI noise model.

the superposition theory, the effect of a voltage/current source on EMI can be analyzed after shorting other voltage sources and disconnecting other current sources. It is found that only $V_{\rm SW1}$ contributes to the CM noise [24] flowing to the attached input and output cables, causing radiated EMI. As a result, $I_{\rm SW2}$ and $I_{\rm SW3}$ can be removed in the model, as shown in Fig. 3.

In Fig. 3, the impedances of capacitors C_X, C_{i1}, C_{i2}, and C_o are assumed to be zero for CM EMI analysis, so $V_{\rm SW1}$ is directly added to the primary winding of the transformer. Also, one terminal of the primary winding is equivalently connected to PGND. The two conductors of both input and output cables can be treated as one for CM noise analysis. The attached power cables behave like an antenna which can be characterized with an equivalent antenna impedance $Z_{\rm Antenna}$ [9], [15], [25] in Fig. 4.

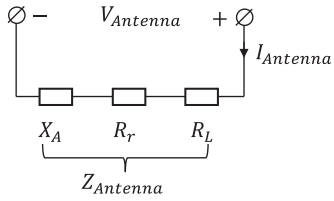

Fig. 4. Equivalent antenna impedance [25].

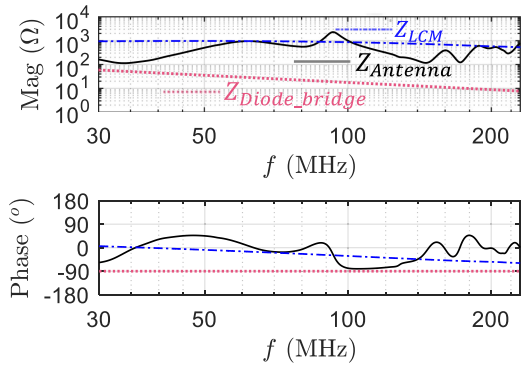

Fig. 5. Extracted impedances of the antenna, CM choke, and diode bridge.

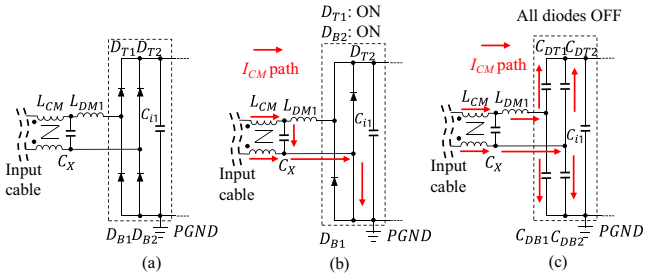

Fig. 6. Impedance of the diode bridge can be ignored for the radiated CM current. (a) Schematic. (b) Two diodes are ON. (c) All diodes are OFF.

R_r is the equivalent radiation resistance, R_L is the loss resistance of the power cables, X_A is the reactance representing the near field energy, so $Z_{\rm Antenna} = R_r + R_L + jX_A$ [25].

The measured impedance $Z_{\rm Antenna}$ of the cable antenna [15] and $Z_{\rm LCM}$ of the CM choke $L_{\rm CM}$ are shown in Fig. 5. It should be noted that based on the antenna theory, the antenna impedance includes the effect of the real ground, so the real ground's effect is included in the antenna impedance $Z_{\rm Antenna}$.

The CM choke uses a Ni-Zn NL16D core from Hitachi, with an outer diameter 8 mm, an inner diameter 4 mm, a thickness 2 mm, and a 9-turn (AWG26) bifilar winding structure. In the concerned frequency range from 30 to 230 MHz (EN55032 3 m class B has the strictest radiated EMI limit in this range), $Z_{\rm LCM}$, which is equivalently in series with $Z_{\rm Antenna}$, is higher or comparable to $Z_{\rm Antenna}$ so it can help reduce the CM currents on the antenna.

For the diode-bridge (Z4DGP406L-HF from Comchip Technology) in Fig. 6(a), when two diodes conduct currents in Fig. 6(b), the CM impedance of the diode bridge is negligible. In Fig. 6(c), when all diodes are OFF, the CM current will flow through diode junction capacitances. Due to the impedance of

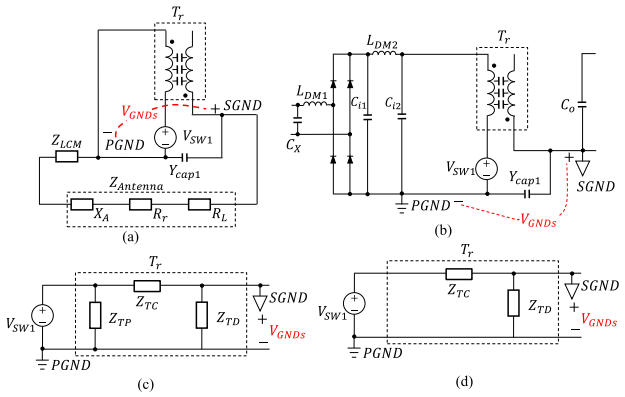

Fig. 7. (a) System EMI model. (b) Extraction of parasitics between PGND and SGND with $L_{\rm CM}$ and cables removed. (c) π model. (d) Reduced model.

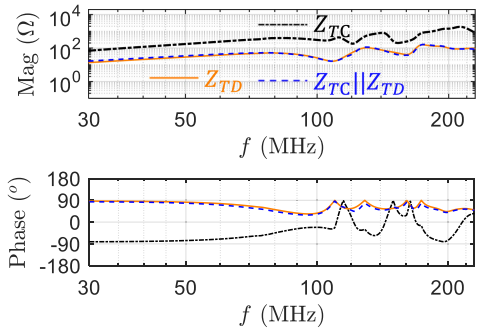

Fig. 8. Extracted impedances.

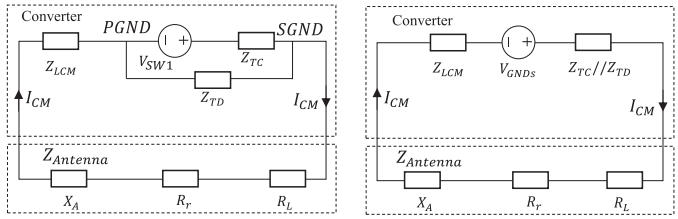

Fig. 9. (a) Preliminary radiated EMI model of the ACF. (b) Reduced model.

DM inductor $L_{\rm DM1}$, two lines may have different CM currents. For the worst scenario, when the CM current only flows through the line without $L_{\rm DM1}$, the impedance $Z_{\rm Diode\_bridge}$ of the diode bridge is the two parallel 45-pF diode junction capacitances. $Z_{\rm Diode\_bridge}$ is much smaller than the impedances of the antenna and $L_{\rm CM}$, as shown in Fig. 5. The impedance of the diode bridge can, therefore, be ignored in the radiated EMI analysis. Also, in Fig. 6(c), since the diode bridge impedance is ignored, the CM current bypasses $L_{\rm DM1}$ via the other line, so $L_{\rm DM1}$ can be ignored.

Based on the abovementioned analysis , the EMI model with transformer parasitics can be simplified to Fig. 7(a) with both the impedances of the diode bridge and $L_{\rm DM1}$ ignored. $V_{\rm GNDs}$ between PGND and SGND is the excitation voltage to drive $L_{\rm CM}$ and antenna for EMI radiation. To investigate $V_{\rm GNDs}$ in Fig. 7(a), $L_{\rm CM}$, input and output cables are removed in Fig. 7(b). Because any parasitics across PGND and SGND may contribute to $V_{\rm GNDs}$, although the impedances of C_{i1}, C_{i2}, C_o, C_X, the diode bridge and the related PCB trace connections are ignored, they may contribute to the parasitic mutual capacitance across PGND and SGND, so they will be kept on the PCB for the parasitic extraction. Because $V_{\rm SW1}$ is the equivalent switching voltage source added to the primary winding of the transformer, and the resultant excitation voltage $V_{\rm GNDs}$ is the voltage difference between PGND and SGND, the circuit including all parasitics between PGND and SGND in Fig. 7(b) can be modeled as a two-port network: the PGND, which is connected to one of the primary winding's two terminals in Fig. 7(b), is the reference ground; the other primary winding's terminal, which is connected to $V_{\rm SW1}$, is the input port, and the SGND is the output port. The output port voltage is, therefore, $V_{\rm GNDs}$. Based on the network theory, a two-port network can be represented with a π network including $Z_{\rm TP}$, $Z_{\rm TD}$, and $Z_{\rm TC}$ in Fig. 7(c). Since $Z_{\rm TP}$ is in parallel with $V_{\rm SW1}$, it can be removed. The network is reduced to Fig. 7(d). $Z_{\rm TD}$ and $Z_{\rm TC}$ can be extracted via S-parameters [15] using the Copper Mountain planar 808/1 vector network analyzer (VNA) and the results are shown in Fig. 8.

In Fig. 8, based on the magnitude and positive phase information, $Z_{\rm TD}$ behaves like an inductive impedance in the whole frequency range from 30 to 230 MHz. $Z_{\rm TD}$ is determined by the transformer parasitics, the impedance of $Y_{\rm cap1}$ and its related parasitic inductance. $Y_{\rm cap1}$ has an surface-mount device (SMD) 1808 package with capacitance 1.5 nF. On the other hand, the phase of $Z_{\rm TC}$ is negative from 30 to 107 MHz, but the polarity changes frequently above 107 MHz. $Z_{\rm TC}$ is much bigger than $Z_{\rm TD}$ below 230 MHz, so the transformer's total CM impedance $Z_{\rm TC}//Z_{\rm TD}$ is mostly determined by $Z_{\rm TD}$ for this converter.

With the transformer model in Fig. 7(d), the radiated EMI model can be developed in Fig. 9(a), where $I_{\rm CM}$ is the CM current flowing through the power cables, causing the radiated EMI. Applying Thevenin equivalence between PGND and SGND, it can be further reduced to Fig. 9(b). $Z_{\rm TC}//Z_{\rm TD}$ is the Thevenin equivalent impedance. It is much smaller than $Z_{\rm LCM}$ and $Z_{\rm Antenna}$ based on Figs. 5 and 8, so it can be ignored.

B. Improved Radiated EMI Model Including Capacitive Couplings

In the experiments, it was found that capacitive couplings play a big role in the radiated EMI. The undesired capacitive couplings exist between conductors with pulsating voltage difference, especially between sensitive nodes and noisy nodes. In order to identify possible capacitive couplings in Fig. 1, components and PCB traces with similar voltage levels are identified as voltage nodes in shaded areas in Fig. 10(a). The explanations of these nodes are in Table I. The capacitive couplings between any two nodes are analyzed in Table II.

The extraction of the impedances $Z_{\rm CAC}$ and $Z_{\rm CAB}$ of $C_{\rm AC}$ and $C_{\rm AB}$ using a two-port VNA is shown in Fig. 10(b). Before the measurement, the calibration was made to the exact measurement points, so no additional test wires are needed to do the measurement. The effect of the gradient voltage on the

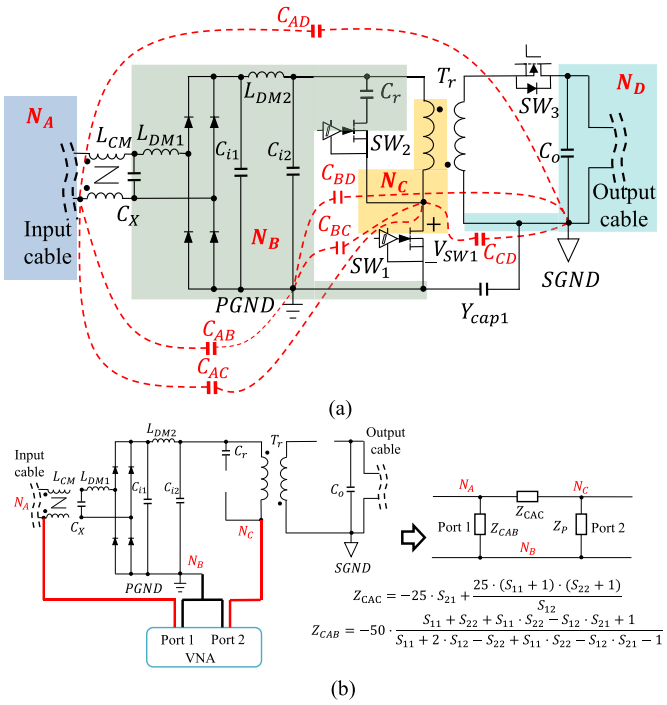

Fig. 10. (a) Identified voltage nodes and capacitive couplings in the ACF. (b) Extraction of C_{AC} and C_{AB}.

TABLE I
IDENTIFIED VOLTAGE NODES

Node	Components and PCB traces with a similar voltage level
N_A	Input cable before CM choke (victim)
N_B	C_X, L_{DM1}, diode bridge, C_{i1}, C_{i2} , L_{DM2}, and dc bus
N_C	Drain of SW_1, source of SW_2, PCB traces and the transformer winding with a gradient voltage
N_D	Output dc bus, C_o, and output cable

transformer primary winding on capacitive couplings is also included in the measurement because the voltage excitation from port 2 is directly added to the primary winding and this voltage is a gradient voltage on the primary winding. It should be noted that, to extract the coupling parasitics due to V_{SW1}, based on the superposition theory, other switching devices SW_2 and SW_3 are removed. The extracted *S*-parameters are converted to a π impedance network [23]. The three impedances of the network correspond to Z_{CAC}, Z_{CAB}, and Z_P. Z_P, which is the impedance between N_C and N_B in Fig. 10(b), is not needed in the EMI model. Other parasitic capacitances can be extracted similarly. C_{AC} and C_{AB} are extracted as 1.05 pF and 0.63 pF. The equivalent parallel capacitance (EPC) of the CM choke is 1.29 pF. C_{CD} and C_{BD} are extracted as 1.59 pF and 3.7 pF with port 1 connected between N_C and N_B, port 2 connected between N_D and N_B, and the transformer removed. Their effects have been included in Z_{TC} and Z_{TD} as discussed in Tabel II. Based on the analysis in Table II, the capacitive coupling C_{AC} between the victim node N_A and the pulsating node N_C is a very important coupling. It should be pointed out that within the radiated EMI frequency range, the voltage along a cable antenna is not constant, so representing the distributed capacitive coupling

TABLE II
CAPACITIVE COUPLINGS BETWEEN CM NODES

	Involved nodes	Analyses about the significance
C_{AC}	N_A & N_C	Couplings from the pulsating node to the victim node can inject noise to the input cable, so it is a critical coupling.
C_{AB}	N_A & N_B	C_{AB} is in parallel with the CM choke, so it may degrade CM choke performance.
C_{AD}	N_A & N_D	C_{AD} is part of the antenna composed of input and output cables; it is determined by the test setup. However, an external capacitance between input and output cables can help reduce the antenna impedance and the radiated EMI.
C_{BC}	N_B & N_C	C_{BC} is in parallel with SW_1, so it does not influence the gain from V_{SW1} to the CM noise and to the radiated EMI.
C_{BD}	N_B & N_D	Effect of C_{BD} has been included in the extracted Z_{TD} in Fig. 7; if its impedance is much bigger than those of Y_{cap1} and the transformer, it has negligible influence.
C_{CD}	N_C & N_D	Effect of C_{CD} has been included in the extracted Z_{TC} in Fig. 7; if its impedance is much larger than that of the transformer, it can be ignored.

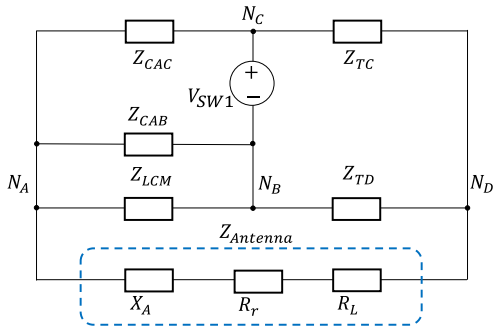

Fig. 11. Radiated EMI model including the capacitive couplings.

between a node and a long cable using a lumped capacitance can give a qualitative analysis but not a quantitative analysis. However, the qualitative analysis can still help identify important couplings and develop techniques to reduce the coupling and the radiated EMI.

The radiated EMI model is improved from Fig. 9(a) to include the impedances of C_{AC} and C_{AB} in Fig. 11. The improved model is a Wheatstone bridge with V_{SW1} as the noise source and the antenna impedance as the load. The output voltage V_{AD} (voltage between nodes N_A and N_D) of the bridge due to the unbalance is the excitation voltage of the antenna. The voltage gain is

$$\frac{V_{AD}}{V_{\mathrm{SW1}}} \approx \left(\frac{Z_{\mathrm{Antenna}}}{Z_{\mathrm{LCM}}//Z_{\mathrm{CAB}}//Z_{\mathrm{CAC}} + Z_{\mathrm{Antenna}}} \right) \times \left(\frac{Z_{\mathrm{LCM}}//Z_{\mathrm{CAB}}}{Z_{\mathrm{LCM}}//Z_{\mathrm{CAB}} + Z_{\mathrm{CAC}}} - \frac{Z_{\mathrm{TD}}}{Z_{\mathrm{TD}} + Z_{\mathrm{TC}}} \right). \quad (1)$$

In (1), the second factor represents the balance condition of the Wheatstone-bridge. Based on the extracted parasitic impedances in Figs. 5 and 8, Fig. 12 shows the results of the second factor. Compared with the balance curve without C_{AC}, i.e., $Z_{\mathrm{TD}}/(Z_{\mathrm{TD}} + Z_{\mathrm{TC}})$ in the same figure, the capacitive coupling C_{AC} introduces more unbalance, so it greatly increases V_{AD} and the radiated EMI.

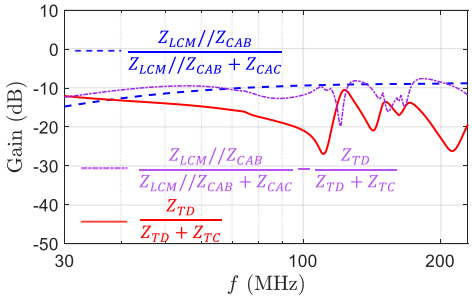

Fig. 12. Capacitive coupling C_{AC} leads to more unbalance.

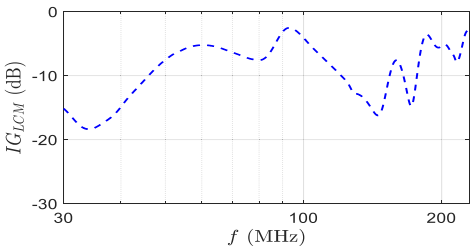

Fig. 13. Calculated insertion gain of the CM choke for the radiated EMI.

C. Experimental Verification

Based on the preliminary radiation model in Fig. 9(b), the radiated power P_r on R_r can be predicted and the radiated maximum electric field intensity $E_{\max}$ at distance r from the converter is given by (2) [9] for this preliminary model

$$E_{\max}=\sqrt{\frac{\eta D_o P_r}{2\pi r^2}}=\sqrt{\frac{\eta D_o}{2\pi r^2}} \times \frac{|V_{\mathrm{GNDs}}|}{|Z_{\mathrm{Antenna}}+Z_{\mathrm{LCM}}+Z_{\mathrm{TC}}//Z_{\mathrm{TD}}|}\sqrt{R_r} \quad (2)$$

where η is the characteristic impedance $120\pi\ \Omega$; D_o is the maximum directivity of the antenna at distance r.

Based on (2), the insertion gain $\mathrm{IG_{LCM}}$ of L_{CM}, which is defined as the ratio of the radiated $E_{\max}$ with L_{CM} to that without L_{CM}, can be derived in the following equation:

$$\mathrm{IG_{LCM}}=\frac{1}{|1+Z_{\mathrm{LCM}}/(Z_{\mathrm{Antenna}}+Z_{\mathrm{TC}}//Z_{\mathrm{TD}})|} \approx \frac{1}{|1+Z_{\mathrm{LCM}}/Z_{\mathrm{Antenna}}|}. \quad (3)$$

From (3), high Z_{LCM} can reduce radiated EMI. Fig. 13 shows the calculated insertion gain based on (3). L_{CM} can reduce radiated EMI by 3–18 dB from 30 to 230 MHz.

The radiated EMI of the ACF is measured in a 3-m semi-anechoic chamber, as shown in Fig. 14, according to the EMI standard EN55032 class B for power adapters. Ferrite beads (Fair-Rite 0431167281) are used on the input cable before the AC plug to isolate the grid from the measurement [15].

Based on the measured EMI without the CM choke and the calculated insertion gain of the CM choke, the radiated EMI with the CM choke is predicted and compared with the measured in Fig. 15. The measured is several dB higher than the predicted above 70 MHz because of the capacitive coupling

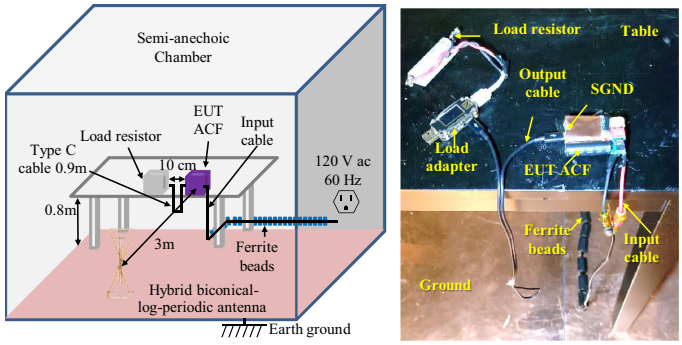

(a) (b)

Fig. 14. (a) Radiated EMI measurement in a semianechoic chamber. (b) Photograph.

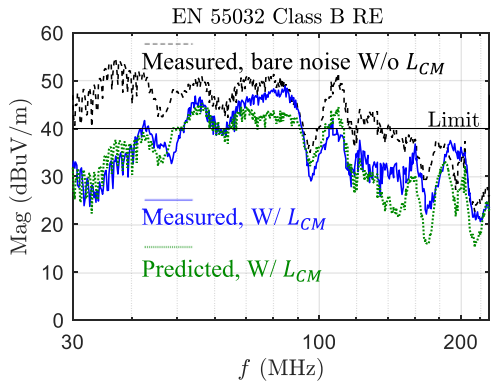

Fig. 15. Comparison of the measured and the predicted radiated EMI.

C_{AC} as analyzed in Section II-B. Furthermore, the radiated EMI cannot meet the EMI limit below 120 MHz.

Based on the analysis in Section II-B, the capacitive coupling C_{AC} should be reduced to reduce the radiated EMI. To validate the impacts of capacitive coupling C_{AC}, an experiment is conducted in Fig. 16. A copper shielding is applied to node N_C with the traces and components including the whole transformer identified in Table I shielded. The shielding is connected to SGND, so the capacitive coupling between N_A and N_C is bypassed to SGND, and the C_{AC} is eliminated. With the shielding, C_{CD} and C_{BC} in Fig. 13(a) are also eliminated. The parasitic capacitance C_{CS} and C_{AS} represent the capacitive couplings between N_C and the shielding, and between shielding and N_A. C_{AS} is in parallel with Z_{Antenna}, so it can help reduce the radiated EMI. C_{CS} is part of Z'_{TC}. C_{BS} between the shielding and N_B is part of Z'_{TD}. The model is shown in Fig. 17. Z'_{TC} and Z'_{TD} can be extracted similar to that of Z_{TC} and Z_{TD} in Fig. 7.

Similar to the extraction of C_{BD} and C_{CD} with the transformer removed, C_{CS} and C_{BS} are extracted as 1.93 pF and 4.7 pF. They are only slightly bigger than C_{CD} and C_{BD}, so Z'_{TC} and Z'_{TD} are close to Z_{TC} and Z_{TD}. It should be pointed out that because the extracted impedance of C_{CS} above 160 MHz is determined by high-order parasitics, the difference between Z'_{TC} and Z_{TC} is bigger above 160 MHz in Fig. 18. The capacitive coupling between the shielding and N_D is shorted so it does not contribute to the radiated EMI. It should be pointed out that, the shielding should be connected to SGND rather than PGND. If the shielding

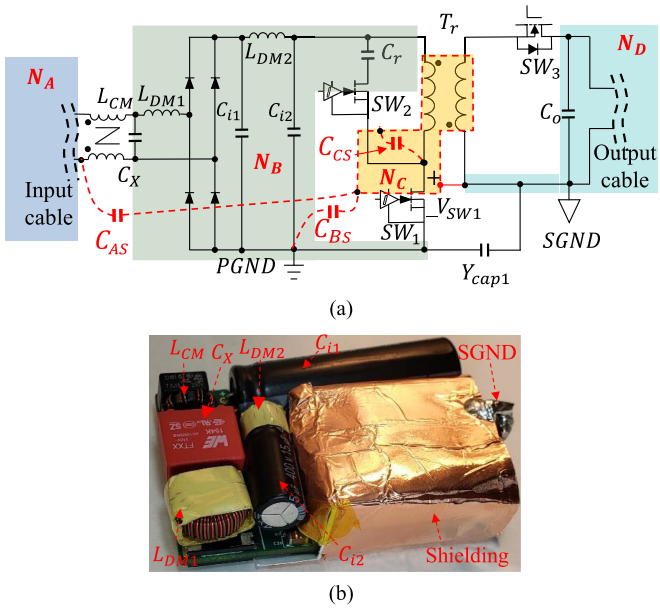

Fig. 16. Applying a shielding to the pulsating node N_C. (a) Circuit. (b) Photograph.

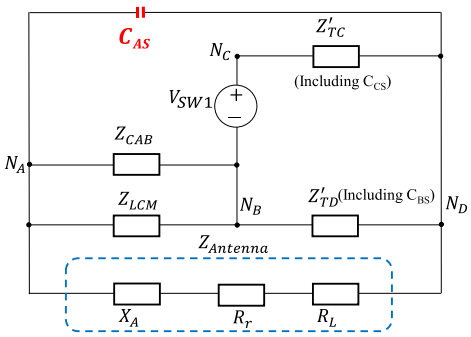

Fig. 17. Radiated EMI model with the node N_C shielded.

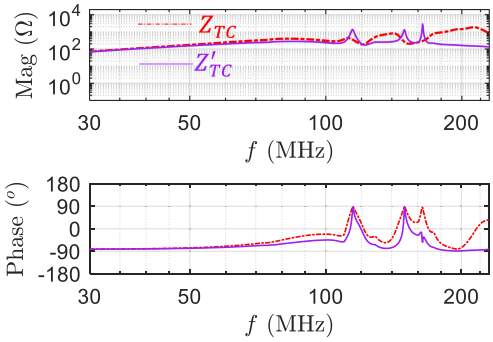

Fig. 18. Comparison of the extracted Z_{TC} and Z'_{TC}.

is connected to PGND, the capacitive couplings between N_A and the shielding can increase C_{AB}, which degrades the performance of the CM choke.

C_{AS} is extracted as 4.38 pF. It is in parallel with the cable antenna, so the parallel impedance is smaller than the antenna impedance above 55 MHz as in Fig. 19. Because the parallel

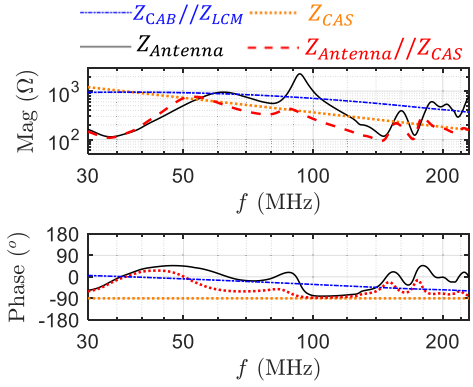

Fig. 19. Impedance comparison.

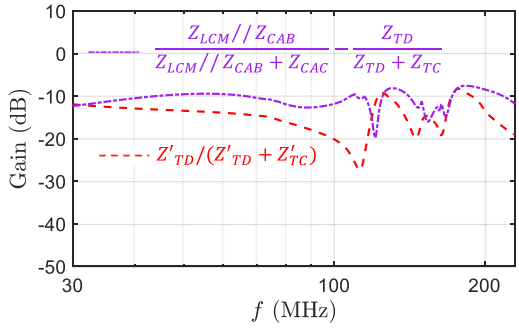

Fig. 20. Comparison of the second factors in (1) and (4).

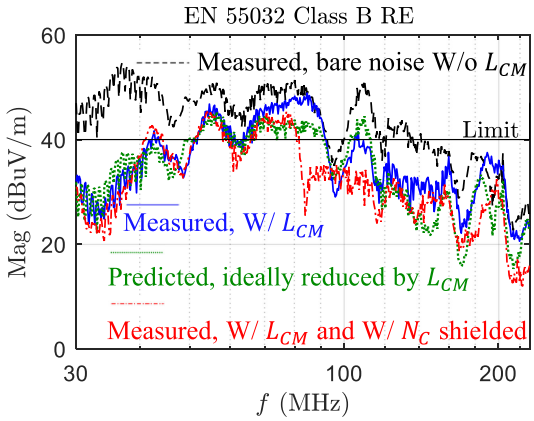

Fig. 21. Measured radiated EMI reduction by shielding N_C.

impedance is smaller than $Z_{\mathrm{CAB}}//Z_{\mathrm{LCM}}$, based on the model in Fig. 17, C_{AS} helps reduce the radiated EMI above 55 MHz.

The voltage gain from V_{SW1} to V_{AD} is

$$\frac{V_{\mathrm{AD}}}{V_{\mathrm{SW1}}} \approx \left(\frac{Z_{\mathrm{Antenna}}//Z_{\mathrm{CAS}}}{Z_{\mathrm{CAB}}//Z_{\mathrm{LCM}}+Z_{\mathrm{Antenna}}//Z_{\mathrm{CAS}}}\right) \times \left(\frac{Z'_{\mathrm{TD}}}{Z'_{\mathrm{TC}}+Z'_{\mathrm{TD}}}\right). \tag{4}$$

Comparing (4) with (1), the first factor in (4) is greatly smaller than that in (1) due to the impedance of C_{AS}, which will be shown later in Fig. 25(a). The second factor in (4) is also smaller than that in (1), as shown in Fig. 20. The measured radiated EMI in Fig. 21 verified this. In Fig. 21, the radiated EMI with

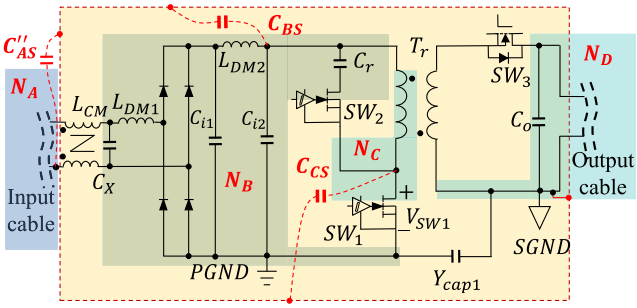

Fig. 22. Applying a shielding to the whole converter.

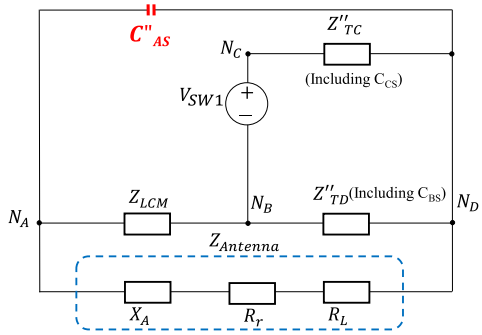

Fig. 23. Radiated EMI model with the whole converter shielded.

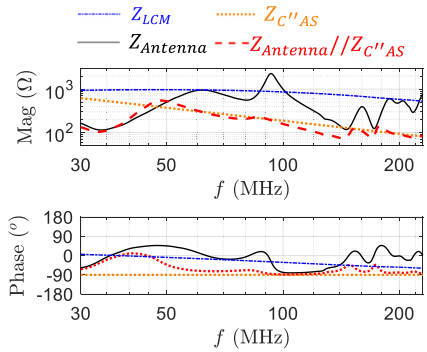

Fig. 24. Impedance comparison.

the shielding applied is even lower than the predicted one with $L_{\rm CM}$ but no capacitive couplings because the shielding not only eliminates the undesired capacitive couplings such as $C_{\rm AC}$ but also introduces desired capacitive coupling such as $C_{\rm AS}$, which helps further reduce the radiated EMI.

However, as shown in Fig. 21, the radiated EMI cannot meet the EMI limit below 80 MHz. It is, therefore, necessary to develop noise reduction techniques to further reduce the radiated EMI.

It should be noted that the total capacitance $C_{\rm AS} + C_{\rm BS} + C_{\rm CS}$ between the shielding, which is grounded to the secondary side, and the converter's primary side is around 11 pF whose impedance is much higher than the transformer's interwinding impedance and the 1.5 nF *Y*-capacitor. The effect of $C_{\rm AS} + C_{\rm BS} + C_{\rm CS}$ on the 50/60 Hz safety leakage current is, therefore, ignored.

III. Techniques to Reduce Capacitive Couplings and Radiated EMI

A. Whole Converter Shielding Technique

Shielding the whole converter with the shielding connected to SGND, as shown in Fig. 22, will have a better performance than shielding N_C because of the following four reasons.

1) $C_{\rm AC}$ is eliminated because the whole converter shielding can bypass the capacitive couplings between N_A and N_C to SGND.
2) $C_{\rm AB}$ is eliminated by the shielding because the shielding bypasses the coupling to SGND so $Z_{\rm LCM}$ is not compromised.
3) $C_{\rm AS}$ ($C''_{\rm AS}$ for this case), which is in parallel with the antenna, is increased.
4) The capacitive coupling $C_{\rm BS}$ between the shielding (SGND) and node N_B (PGND) is increased to help further reduce the high frequency radiated EMI.

For 3) and 4) mentioned above, compared with the partial shielding in Fig. 16, the whole converter shielding has a bigger shielding area, is closer to input cable N_A, and covers much more area of N_B, including $C_{\rm i1}$, $C_{\rm i2}$, $L_{\rm DM1}$, $L_{\rm DM2}$, and the diode bridge, than the partial shielding, so it has a bigger $C_{\rm BS}$ and $C''_{\rm AS} > C_{\rm AS}$. The parasitics are extracted as $C_{\rm CS} = 1.93$ pF, $C''_{\rm AS} = 8.58$ pF, and $C_{\rm BS} = 11.3$ pF. The radiated EMI model is in Fig. 23. Compared with Fig. 17, $Z''_{\rm TD}$ is smaller than $Z'_{\rm TD}$ $Z_{\rm LCM}$ is bigger than $Z_{\rm LCM}//Z_{\rm CAB}$ and $C''_{\rm AS}$ is bigger than $C_{\rm AS}$.

All of these help greatly reduce radiated EMI. In Fig. 24, the impedance of the CM choke is much bigger than the parallel impedance of antenna and $C''_{\rm AS}$ in the whole frequency range. The voltage gain is

$$\frac{V_{\rm AD}}{V_{\rm SW1}} \approx \left(\frac{Z_{\rm Antenna}//Z_{C''_{\rm AS}}}{Z_{\rm LCM} + Z_{\rm Antenna}//Z_{C''_{\rm AS}}}\right)\left(\frac{Z''_{\rm TD}}{Z''_{\rm TC} + Z''_{\rm TD}}\right). \tag{5}$$

Because of $C''_{\rm AS}$, the first factor in (5) is greatly reduced especially above 50 MHz, as shown in Fig. 25(a). The second factor is also reduced. Based on (1), (4), and (5), the predicted voltage gains without shielding, with N_C shielded, and with the whole converter shielded are compared in Fig. 25(b). The whole converter shielding gives the lowest voltage gain as predicted by (5).

The measured EMI is shown in Fig. 26. It is shown that, with the whole converter shielding, the radiated EMI can be further reduced above 50 MHz compared with the N_C shielding. This validates the analysis. It should be noted that based on the measurements, the shielding does not sacrifice the converter efficiency (93%) because the eddy current due to the leakage magnetic field of the transformer is very small. Similar to the shielding in Fig. 16, the total capacitance $C''_{\rm AS} + C_{\rm BS} + C_{\rm CS}$ between the shielding, which is grounded to SGND, and the converter's primary side is around 21.8 pF whose impedance is much higher than the transformer's interwinding impedance and the 1.5 nF *Y*-capacitor. Its effect on the 50/60 Hz safety leakage current is, therefore, ignorable.

The predicted radiated EMI reduction in Fig. 25 is larger than the measured in Fig. 26 because, as pointed out in Section II-B,

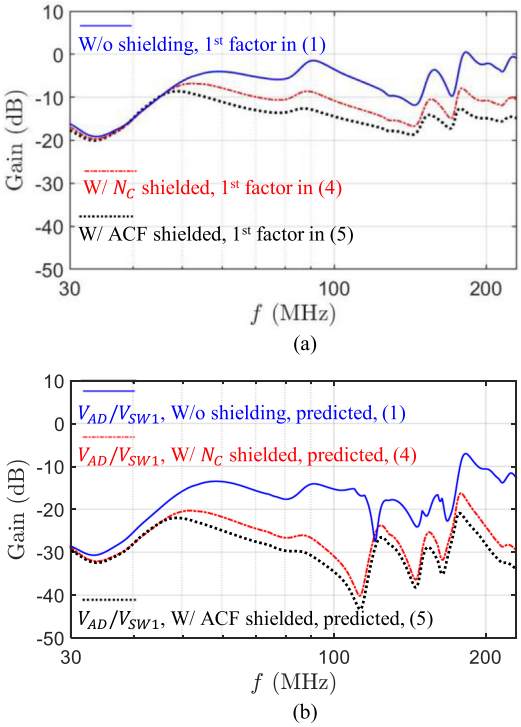

Fig. 25. Comparison of the predicted voltage gains from (1), (4), and (5). (a) Comparison of the first factors. (b) Comparison of the predicted voltage gains.

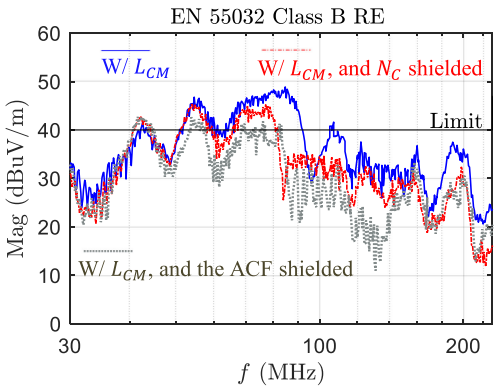

Fig. 26. Radiated EMI reduction by shielding the whole converter.

the model in Fig. 23 is based on the lumped instead of distributed capacitive couplings, so it gives a qualitative view but not a quantitative view.

B. Improved Whole Converter Shielding Technique

Since the whole converter shielding and the increased $C_{\rm AS}$ can help reduce the radiated EMI, it is appropriate to add a small capacitor $Y_{\rm cap2}$ from N_A to the shielding, as shown in Fig. 27(a) and (b), to increase $C_{\rm AS}$ on purpose. $Y_{\rm cap2}$, $L_{\rm CM}$, and $Y_{\rm cap1}$ form a capacitor-inductor-capacitor (CLC) CM EMI filter. $Y_{\rm cap2}$ is connected to SGND via the shielding which has a very small inductance, so it has a good HF performance.

The impedance of $Y_{\rm cap2}$ should be as small as possible to reduce the excitation voltage on the antenna. At the same time,

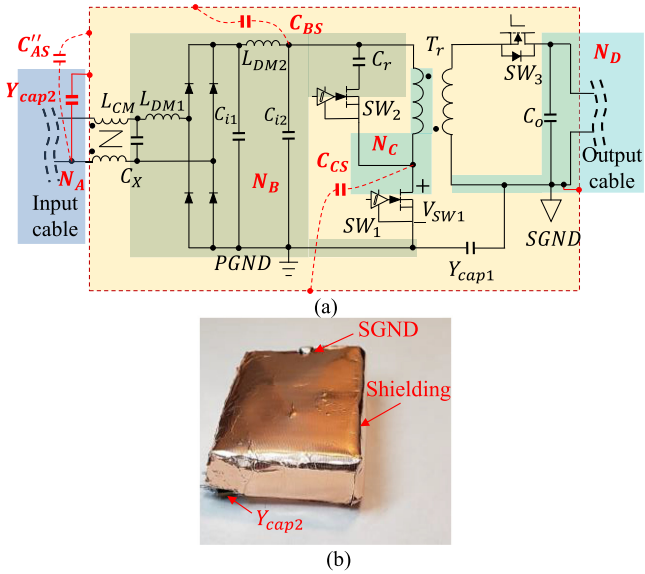

Fig. 27. Proposed CLC shielding CM filter technique. (a) Circuit. (b) Photograph.

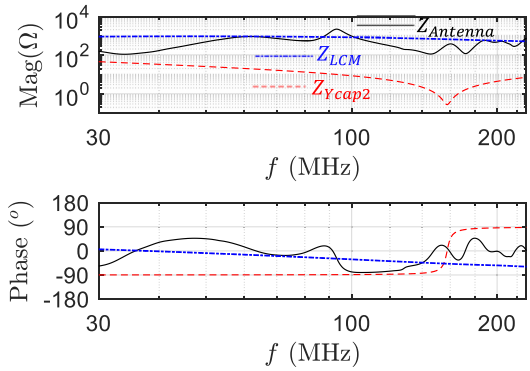

Fig. 28. Impedance comparison.

$Y_{\rm cap1}$ has been designed to meet the conductive EMI standard, so it should be not changed. Because both $Y_{\rm cap1}$ and $Y_{\rm cap2}$ generate leakage current from the AC line to DC output, $Y_{\rm cap2}$ should be kept small to meet safety requirements. In HF range, the equivalent series inductance of a *Y*-capacitor is significantly influenced by the packaging technique. Therefore, a small form factor SMD 1808, 100 pF safety capacitor is selected. The impedance $Z_{Y\rm cap2}$ including both the impedances of $Y_{\rm cap2}$ and the shielding from N_A to N_D is much smaller than other impedances above 50 MHz in Fig. 28. Because of this, the excitation voltage of the antenna, thus the radiated EMI can be greatly reduced.

The measured radiated EMI compared with the other three cases is shown in Fig. 29. In Fig. 29, the radiated EMI is greatly reduced from 40 to 120 MHz compared with that without $Y_{\rm cap2}$. It can meet the radiated EMI limit.

When implementing the proposed techniques, a full converter shielding grounded to SGND with $Y_{\rm cap2}$ connected to the shielding gives the best radiated EMI reduction. Fig. 30 shows the comparison of the measured radiated EMI with different $Y_{\rm cap2}$ connection patterns. In the first case, without the shielding applied, $Y_{\rm cap2}$ is directly connected to SGND via a piece of wire.

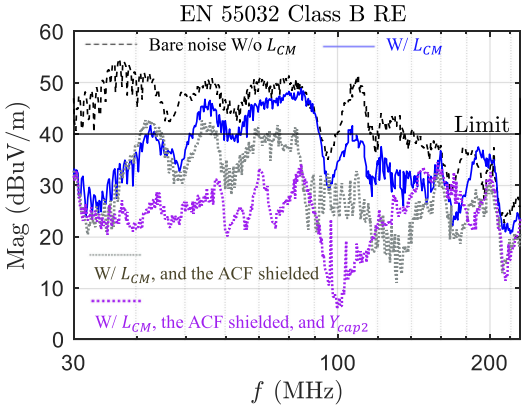

Fig. 29. Radiated EMI with the whole converter shielding and Y_{cap2}.

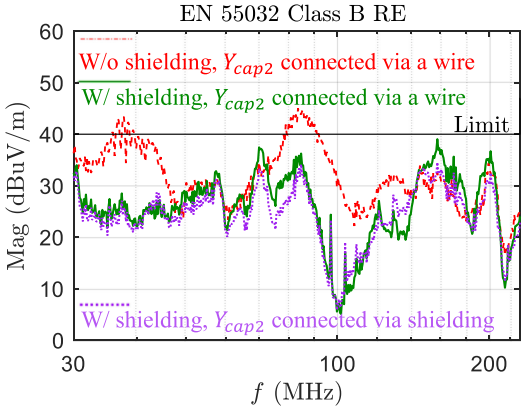

Fig. 30. Radiated EMI comparison of different Y_{cap2} connection patterns.

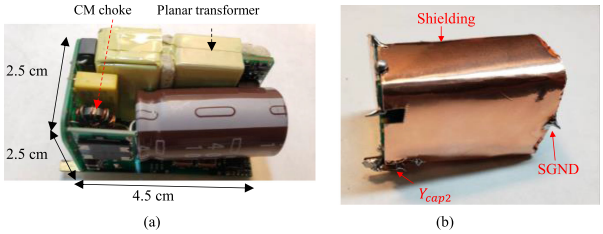

Fig. 31. Different ACF prototype: (a) photograph (b) with a shielding and Y_{cap2}.

Due to the capacitive couplings C_{AB} and C_{AC} as analyzed in Section II, the CLC filter (Y_{cap2}–L_{CM}–Y_{cap1})'s performance is degraded, so it cannot meet the radiated EMI limit. In the second case, the shielding is applied, but Y_{cap2} is directly connected to SGND via a piece of wire instead of via the shielding. The radiated EMI is much lower than the first case. In the third case, Y_{cap2} is connected to SGND via the shielding. It leads to the lowest radiated EMI to meet the EMI limit with enough margin.

The proposed techniques are insensitive to different prototypes because of the following: 1) the proposed techniques can eliminate the most important capacitive couplings between N_A and N_C; and 2) the parasitic capacitance C_{AS} between the shielding and N_A can reduce the radiation because it is in parallel with the cable antenna. Fig. 31(a) shows the proposed techniques applied to another ACF prototype, which has different structures and dimensions from the one in Fig. 1(b). The measured radiated EMI in Fig. 32 shows that the proposed techniques are very effective.

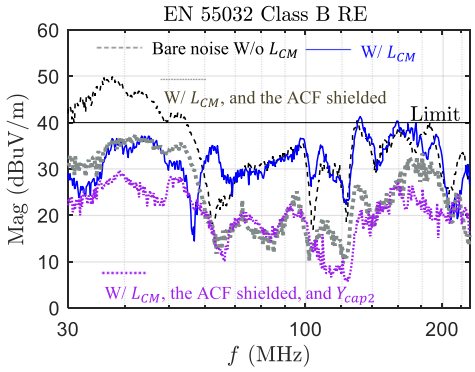

Fig. 32. Proposed techniques reduce radiated EMI regardless of different prototypes.

IV. Conclusion

This article first developed a radiated EMI model for an ACF converter employing GaN switching devices. It was found that, for the radiated EMI analysis, the switching transformer and the parasitic impedances between the primary and secondary sides can be modeled with two impedances; the impedance of a diode bridge can be ignored no matter it is in ON or OFF status; the capacitive couplings between pulsating voltage nodes and the input and output cables are critical to radiated EMI. Based on the developed model, an improved whole converter shielding technique was proposed to greatly reduce the capacitive couplings and the radiated EMI. Both theoretical analyses and experiments were conducted to validate the proposed modeling and EMI reduction techniques.

References

[1] X. Huang, Z. Liu, Q. Li, and F. C. Lee, "Evaluation and application of 600 V GaN HEMT in cascode structure," *IEEE Trans. Power Electron.*, vol. 29, no. 5, pp. 2453–2461, May 2014.

[2] X. Lyu, Y. Li, D. Cao, S. Jiang, and C. Nan, "Comparison of GaN based switched-tank converter and cascaded voltage divider," in *Proc. IEEE 5th Workshop Wide Bandgap Power Devices Appl.*, Albuquerque, NM, USA, Oct./Nov. 2017, pp. 158–164.

[3] B. Li, Q. Li, F. C. Lee, Z. Liu, and Y. Yang, "A high-efficiency high-density wide-bandgap device-based bidirectional on-board charger," *IEEE J. Emerg. Sel. Topics Power Electron.*, vol. 6, no. 3, pp. 1627–1636, Sep. 2018.

[4] S. Zhao *et al.*, "Adaptive multi-level active gate drivers for SiC power devices," *IEEE Trans. Power Electron.*, vol. 35, no. 2, pp. 1882–1898, Feb. 2020.

[5] B. Zhang and S. Wang, "A survey of EMI research in power electronics systems with wide bandgap semiconductor devices," *IEEE J. Emerg. Sel. Topics Power Electron.*, vol. 8, no. 1, pp. 626–643, Mar. 2020.

[6] X. Huang, J. Feng, W. Du, F. C. Lee, and Q. Li, "Design consideration of MHz active clamp flyback converter with GaN devices for low power adapter application," in *Proc. IEEE Appl. Power Electron. Conf. Expo.*, Long Beach, CA, USA, Mar. 2016, pp. 2334–2341.

[7] L. Xue and J. Zhang, "Highly efficient secondary-resonant active clamp flyback converter," *IEEE Trans. Ind. Electron.*, vol. 65, no. 2, pp. 1235–1243, Feb. 2018.

[8] F. C. Lee, "Keynote 1: Is GaN a Game Changing Device?" in *Proc. 16th Int. Power Electron. Motion Control Conf. Expo.*, Antalya, Turkey, Sep. 2014, pp. 8–14.

[9] Y. Zhang, S. Wang, and Y. Chu, "Investigation of radiated electromagnetic interference for an isolated high-frequency DC–DC power converter with power cables," *IEEE Trans. Power Electron.*, vol. 34, no. 10, pp. 9632–9643, Oct. 2019.

[10] J. Yao *et al.*, "Modeling and reduction of radiated common mode current in flyback converters," in *Proc. IEEE Energy Convers. Congr. Expo.*, Portland, OR, USA, Sep. 2018, pp. 6613–6620.

[11] Y. Zhang, S. Wang, and Y. Chu, "Analysis and comparison of the radiated electromagnetic interference generated by power converters with Si MOSFETs and GaN HEMTs," *IEEE Trans. Power Electron.*, vol. 35, no. 8, pp. 8050–8062, Aug. 2020.

[12] S. Wang, F. C. Lee, W. G. Odendaal, and J. D. v. Wyk, "Improvement of EMI filter performance with parasitic coupling cancellation," *IEEE Trans. Power Electron.*, vol. 20, no. 5, pp. 1221–1228, Sep. 2005.

[13] J. Yao *et al.*, "Measurement techniques of CM currents, impedance and voltages for radiated EMI in isolated power converters," in *Proc. IEEE Symp. Electromagn. Compat., Signal Integrity Power Integrity*, Long Beach, CA, USA, Aug. 2018, pp. 438–443.

[14] J. Yao, Y. Li, H. Zhao, and S. Wang, "Design of CM inductor based on core loss for radiated EMI reduction in power converters," in *Proc. IEEE Appl. Power Electron. Conf. Expo*., Anaheim, CA, USA, USA, Mar. 2019, pp. 2673–2680.

[15] J. Yao, S. Wang, and H. Zhao, "Measurement techniques of common mode currents, voltages, and impedances in a flyback converter for radiated EMI diagnosis," *IEEE Trans. Electromagn. Compat.*, vol. 61, no. 6, pp. 1997–2005, Dec. 2019.

[16] H. Zhao, J. Yao, and S. Wang, "A universal DM/CM physical model for power transformer EMI analysis within both conducted and radiated frequency ranges," in *Proc. IEEE Energy Convers. Congr. Expo.*, Portland, OR, USA, Sep. 2018, pp. 6592–6599.

[17] S. Wang, F. C. Lee, and J. D. v. Wyk, "Inductor winding capacitance cancellation using mutual capacitance concept for noise reduction application," *IEEE Trans. Electromagn. Compat.*, vol. 48, no. 2, pp. 311–318, May 2006.

[18] S. Wang, F. C. Lee, J. D. V. Wyk, and J. D. V. Wyk, "A study of integration of parasitic cancellation techniques for EMI filter design with discrete components," *IEEE Trans. Power Electron.*, vol. 23, no. 6, pp. 3094–3102, Nov. 2008.

[19] Y. Liu *et al.*, "FEM modelling of three-phase common mode choke for performance evaluation," in *Proc. Asia Pac. Int. Symp. Electromagn. Compat.*, Shenzhen, China, 2016, pp. 96–99.

[20] S. Wang and F. C. Lee, "Analysis and applications of parasitic capacitance cancellation techniques for EMI suppression," *IEEE Trans. Ind. Electron.*, vol. 57, no. 9, pp. 3109–3117, Sep. 2010.

[21] S. Wang, Y. Y. Maillet, F. Wang, R. Lai, F. Luo, and D. Boroyevich, "Parasitic effects of grounding paths on common-mode EMI Filter's performance in power electronics systems," *IEEE Trans. Ind. Electron.*, vol. 57, no. 9, pp. 3050–3059, Sep. 2010.

[22] F. Costa, C. Gautier, B. Revol, J. Genoulaz, and B. Démoulin, "Modeling of the near-field electromagnetic radiation of power cables in automotives or aeronautics," *IEEE Trans. Power Electron.*, vol. 28, no. 10, pp. 4580–4593, Oct. 2013.

[23] S. Wang, F. C. Lee, and W. G. Odendaal, "Characterization and parasitic extraction of EMI filters using scattering parameters," *IEEE Trans. Power Electron.*, vol. 20, no. 2, pp. 502–510, Mar. 2005.

[24] Y. Li, S. Wang, H. Sheng, and S. Lakshmikanthan, "Investigate and reduce capacitive couplings in a flyback adapter with a DC-bus filter to reduce EMI," *IEEE Trans. Power Electron.*, vol. 35, no. 7, pp. 6963–6973, Jul. 2020.

[25] C. A. Balanis, *Antenna Theory: Analysis and Design*, 3rd ed. Hoboken, NJ, USA: Wiley, 2016.

Juntao Yao (Student Member, IEEE) received the B.S. and M.S. degrees in electrical engineering from Wuhan University, Wuhan, China, in 2013 and 2016, respectively. He is currently working toward the Ph.D. degree with the University of Florida, Gainesville, FL, USA.

He has authored or coauthored more than ten IEEE journal and conference papers and holds one pending U.S. patent and nine issued Chinese patents. His research interests include power electronics, electromagnetic interference (EMI), and magnetic components.

Yiming Li (Student Member, IEEE) received the B.S.E.E. degree in electrical engineering from Zhejiang University, Zhejiang, China, in 2015, and the Ph.D. degree in electrical engineering from the University of Florida, Gainesville, FL, USA, in 2019.

He joined Monolithic Power Systems (MPS), as a Senior Application Engineer in 2020. His research interests include electromagnetic interference and compatibility in power electronic systems. He is also studying on transformer and electromagnetic interference filter design and optimization for switching mode power supplies. He has authored and coauthored more than 18 IEEE journal and conference papers since 2017.

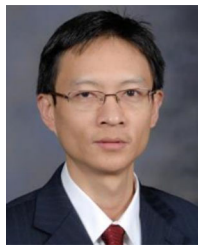

Shuo Wang (Fellow, IEEE) received the Ph.D. degree in electrical engineering from Virginia Tech, Blacksburg, VA, USA, in 2005.

He is currently a Full Professor with the Department of Electrical and Computer Engineering, University of Florida, Gainesville, FL, USA. He has authored or coauthored more than 200 IEEE journal and conference papers and holds around 30 pending/issued U.S./international patents.

Dr. Wang was the recipient of the Best Transaction Paper Award from the IEEE Power Electronics Society in 2006 and two William M. Portnoy Awards for the papers published in the IEEE Industry Applications Society, in 2004 and 2012, and the prestigious National Science Foundation CAREER Award, in 2012. He is currently an Associate Editor for the IEEE TRANSACTIONS ON INDUSTRY APPLICATIONS and IEEE TRANSACTIONS ON ELECTROMAGNETIC COMPATIBILITY. He was a Technical Program Co-Chair for IEEE 2014 International Electric Vehicle Conference.

Xiucheng Huang received the B.S. and M.S. degree in electrical engineering from Zhejiang University, Hangzhou, China, in 2008 and 2011, respectively, and the Ph.D. degree from Virginia Tech, Blacksburg, VA, USA, in 2016.

He is the Senior Director of Application Engineer of Navitas Semiconductor Inc., since 2016. His main research interests include gallium nitride semiconductor devices, high-frequency high density power conversion, soft-switching technique, EMI reduction technique, and power architecture. He has issued three U.S. patents and two Chinese patents, authored or coauthored two book chapters, nine journal papers, and 25 conference papers on IEEE Society.

Xiaofeng Lyu (Member, IEEE) received the B.S. degree from Nanjing University of Aeronautics and Astronautics (NUAA), Nanjing, China, in 2010, and the M.S. degree in power electronics from Zhejiang University (ZJU), Hangzhou, China, in 2013, and the Ph.D. degree from North Dakota State University (NDSU), Fargo, ND, USA, in 2017.

He was with the General Electric (GE) Shanghai, Shanghai, China, Joulwatt Hangzhou, Hangzhou, China, and John Deere Electronic Solutions (JDES), Fargo, ND, USA. He is currently a Staff Applications Engineer with the Navitas Semiconductor, Inc., Los Angeles, CA, USA. His research interests include SiC high-density inverters, switched-tank converter for data center, multilevel converters, LED drivers, and ACF GaN adapters.